Regular Article

PHYSICAL CHEMISTRY RESEARCH
Published by the
Iranian Chemical Society
www.physchemres.org
info@physchemres.org

***Phys. Chem. Res.**, Vol. 7, No. 2, 235-243, June 2019*
DOI: 10.22036/pcr.2019.153980.1555

Influence of Surface Heterogeneities on Complexation of Ethylene with Active Sites of NiMCM-41 Nanocatalyst: A Density Functional Theory Study

M. Ghambarian[a], M. Ghashghaee[a,b,*], Z. Azizi[a,c,*] and M. Balar[c,d]

[a]*Gas Conversion Department, Faculty of Petrochemicals, Iran Polymer and Petrochemical Institute, P. O. Box: 14975-112, Tehran, Iran*
[b]*Faculty of Petrochemicals, Iran Polymer and Petrochemical Institute, P. O. Box: 14975-112, Tehran, Iran*
[c]*Department of Chemistry, Karaj Branch, Islamic Azad University, P. O. Box: 31485-313, Karaj, Iran*
[d]*Young Researchers and Elite Club, Karaj Branch, Islamic Azad University, Karaj, Iran*
(Received 27 October 2018, Accepted 17 January 2019)

Consecutive adsorption of ethylene molecules on different nanoclusters, as representatives of the active sites of NiMCM-41 catalyst, was investigated through studying the structural, topological, and energetic properties at the B3LYP/6-311+G* and M06/Def2-TZVP levels of theory. The dimeric adsorption of the ethylene molecules was found to be exothermic on all sites (adsorption enthalpies ranging from -54.7 to -13.1 kcal mol^{-1} at M06/Def2-TZVP) with the most favorable adsorption on 2T while being non-spontaneous on 5T sites. The π complexation led to the positive total charge on the adsorptive molecules, lengthening the Ni-O and C=C distances, and reducing the O-Ni-O angles, with the smallest changes on 2T and the largest alterations on 4T and 5T. The QTAIM analysis revealed closed-shell interactions between the nickel ion and the olefinic bond. The calculated HOMO-LUMO gaps were attributed to the highest and lowest reactivities of the adsorption complexes formed on 2T and 5T (4.22 and 3.11 eV at B3LYP/6-311+G*), respectively. The results presented highlighted the importance of a systematic study on adsorption steps on different active sites of transition metal catalysts.

Keywords: Ethylene, Adsorption, Nickel, MCM-41, DFT

INTRODUCTION

Light olefins (ethylene, propylene, and butene), being industrially produced by steam cracking [1-4], catalytic cracking [5-6], and dehydrogenation [7-9], constitute the main building blocks for the polymer and petrochemical industries. The demand for short-chain (C4-C8) linear alpha olefins is currently growing faster than that for larger alkenes (C10+) [10-11]. This makes the interconversion technologies quite necessary to bridge the gap between the supply and demand [12-14]. On the other hand, nickel-incorporated materials are deemed as well-known catalysts for effective dimerization [15] or oligomerization [16] of olefins. That is why a lot of research is still being performed on these catalysts. The large ordered channels of MCM-41 have shown highly efficient for oligomerization of ethylene on the internally exchanged nickel ions [17]. The same pathway most possibly relates to the gas-phase transformation of ethylene to propylene over Ni-MCM-41 catalysts [18], which is postulated to commence from a dimerization reaction. Layered nickel-silicate species [19] and three-coordinated Ni^{2+} cations at the 5-membered rings of phyllosilicate walls of NiMCM-41 [20] have been proposed to be the active sites of the reaction.

The metallacycle mechanism is one of the accepted reaction cycles suggested for the dimerization and oligomerization of ethylene over nickel-incorporated catalysts [15]. This is a rational mechanism taking into account that the these catalysts do not need any co-catalyst

*Corresponding authors. E-mail: m.ghashghaee@ippi.ac.ir; zahra.azizi@kiau.ac.ir

to form the activating metal-alkyl species as normally required in homogeneous catalysis [21]. The formation of the active species from a pre-catalyst in these materials is an interesting yet less understood subject. Molecular simulation is an ideal means to address such challenge [9, 16,22-25]. To the best of our knowledge, very scant attention has been paid so far to obtain molecular insights into the above-mentioned system. There exist several theoretical reports on the interactions of Ni^{2+} with models of aluminosilicates [21], none of them concerns to the MCM-41 material. Recently, the molecular heterogeneities of the digrafted Ni^{2+} moieties exchanged into the defect models of MCM-41 were investigated computationally [26] where the 2-membered ring (2MR) and 5MR nickel-siloxane structures were concluded to be the least and the most favorable sites to form, respectively. There is still ample room for making progress in mechanistic understanding, however. More specifically, no theoretical studies dealing with the adsorption stage of the reactions and the molecular-level interactions at the local surface heterogeneities of the nickel sites in MCM-41 catalysts through π complexation have been implemented or, at least, reported in the literature. This paper is then the first demonstration of the relative adsorption properties of one or two molecules of ethylene over different nanoclusters of the NiMCM-41 pre-catalyst within a density functional theory (DFT) framework.

COMPUTATIONAL METHOD

Two molecules of ethylene were adsorbed consecutively on the pre-optimized clusters of NiMCM-41. A two-step optimization procedure was then employed. First, the adsorption sites of the NiMCM-41 pre-catalyst were optimized, followed by the adsorption of ethylene molecule (s) implemented by relaxing the organic part, the nickel ion, and the nearest interacting oxygen atoms to include plausible effects on the skeletal vibrations due to the adsorption. The details of the computations for obtaining the nano-cluster geometries of the active sites can be found elsewhere [26]. For short, the cluster modeling approach applied in several previous studies [16,27] was adopted in which all of the broken bonds at the boundaries of the silicate molecular clusters were terminated by hydrogen atoms placed in the same direction as would be observed in a perfect crystal for the next silicon atom removed from the cluster. The size of the final NiMCM-41 clusters ranged from a 2T to a 6T unit. The corresponding adsorbed structures are referred to herein as M*x*T or D*x*T clusters in which *x* refers to the number of T atoms and M or D signifies the monomeric or dimeric adsorption of ethylene on the investigated sites.

The adsorption geometries were optimized using the two hybrid functionals of B3LYP [28] and M06 [29], respectively, coupled with the 6-31+G* [30] and Def2-TZVP [31] basis sets. These methods are known to yield reliable data for both oxides and metal clusters; e.g., transition metal-exchanged materials [9,32-33]. Frequency calculations were implemented using the B3LYP/6-311+G* [34] and M06/Def2-TZVP methods, respectively. The atomic charges were estimated through the natural bond orbital (NBO) calculations. The enthalpy (ΔH_{ads}), entropy (ΔS_{ads}) and free energy (ΔG_{ads}) changes upon adsorption were calculated for the following reactions:

$$[O_2Si]\text{-}O_2Ni + C_2H_4 \rightarrow [O_2Si]\text{-}O_2Ni\ldots C_2H_4 \quad (1)$$

$$[O_2Si]\text{-}O_2Ni\ldots C_2H_4 + C_2H_4 \rightarrow [O_2Si]\text{-}O_2Ni\ldots 2(C_2H_4) \quad (2)$$

The calculations of NBO population and the quantum theory of atoms in molecules (QTAIM) were implemented at the two levels of theory used for the frequency calculation. For the sake of brevity, hereinafter, the two methods (B3LYP/6-311+G*// B3LYP/6-31+G* and M06/Def2-TZVP) will be referred as L1 and L2, respectively. The computations were conducted using NWChem 6.5 [35] and Multiwfn 3.3.8 [36]. Finally, the graphical outputs were generated by the molecular visualization program Mercury 3.3 [37].

RESULTS AND DISCUSSION

The optimized adsorption structures at the L2 level of theory are shown in Fig. 1. As illustrated, ethylene could be stabilized through η^2(C=C) adsorption on all active sites in both monomeric and dimeric states as also

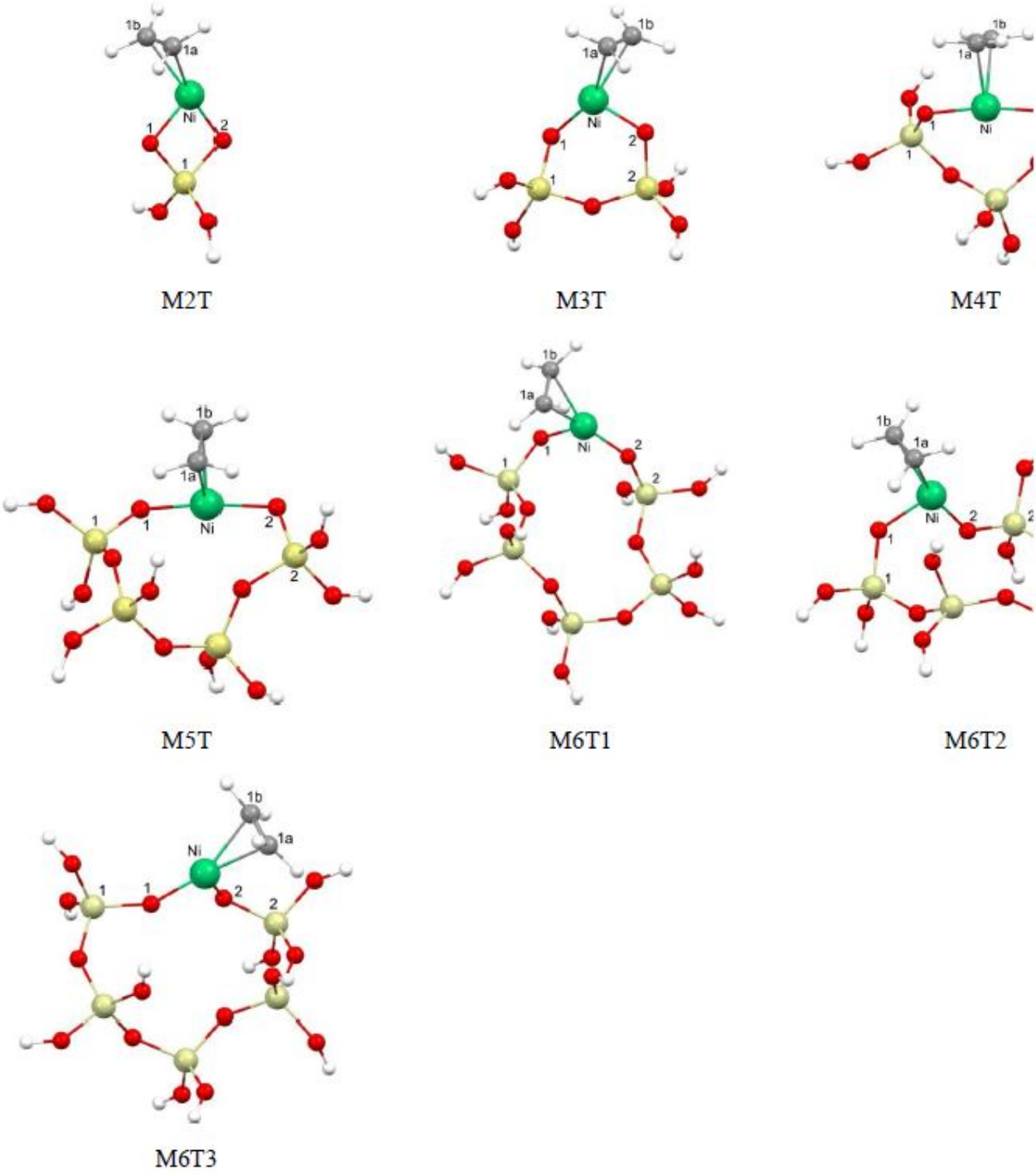

Fig. 1. The optimized geometries of the adsorption complexes on the active sites of NiMCM-41 where the darker (red) spheres represent the framework oxygen atoms, the plain (yellow) bigger balls are silicon atoms, the plain grey spheres represent carbon atoms, and the small white balls are terminal hydrogen atoms. The largest (green) ball represents nickel. Please refer to the online version for references to color.

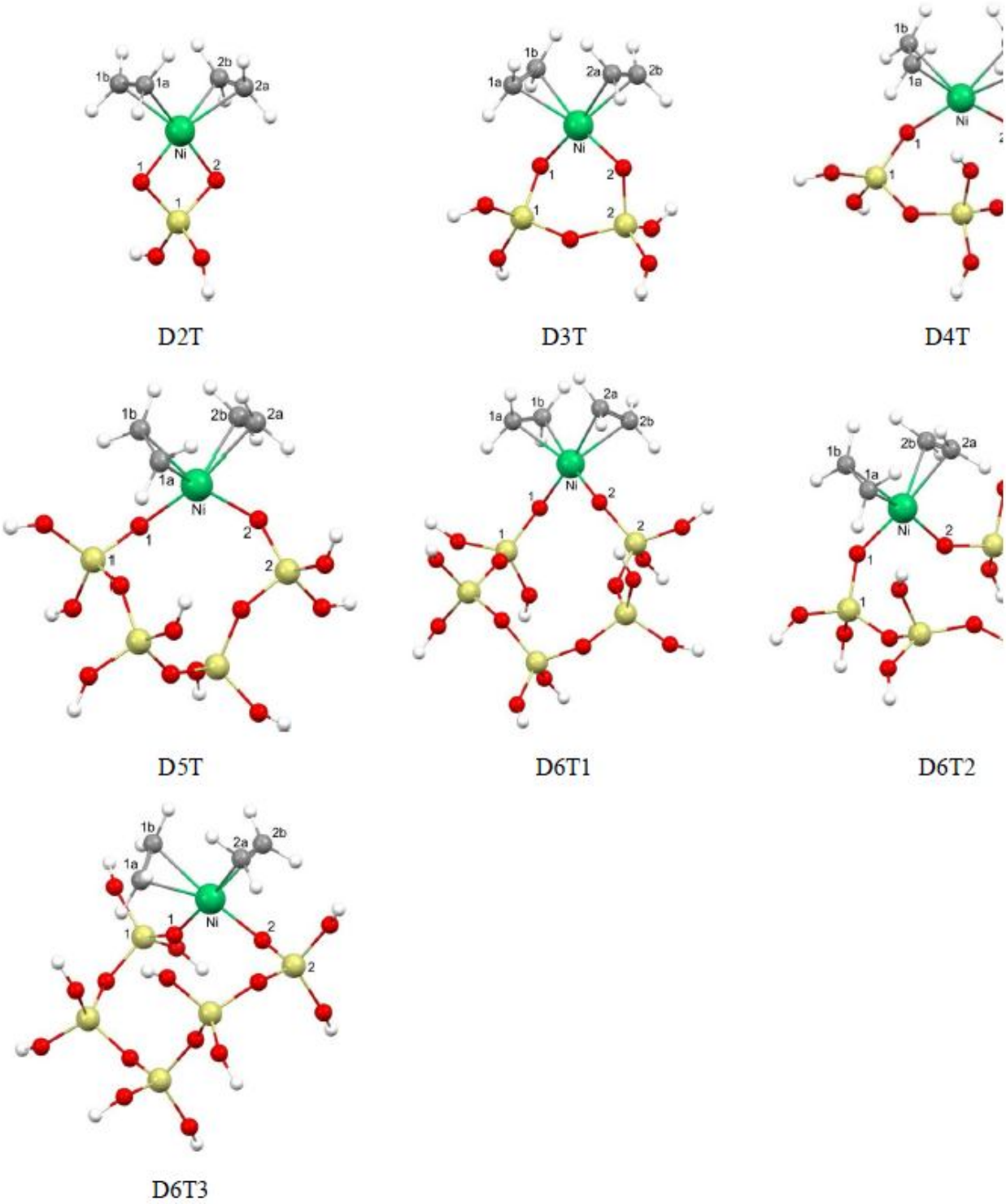

Fig. 1. Continued.

Table 1. The Enthalpy (kcal mol^{-1}), Entropy (cal mol^{-1} K^{-1}), and Gibbs Free Energy (kcal mol^{-1}) Changes upon Adsorption at L1 and L2 (Please See the Corresponding Reactions and Definitions in the Text) at 298 K

	ΔH_{ads}		ΔS_{ads}		ΔG_{ads}	
Cluster	L1	L2	L1	L2	L1	L2
M2T	-28.4	-32.4	-39.0	-38.5	-16.8	-20.9
M3T	-21.1	-24.6	-39.2	-40.3	-9.4	-12.6
M4T	-31.0	-35.7	-38.1	-42.6	-19.6	-23.0
M5T	-29.6	-32.4	-44.8	-38.3	-16.2	-21.0
M6T1	-17.4	-23.9	-31.9	-49.4	-7.8	-9.2
M6T2	-20.9	-25.7	-43.9	-40.9	-7.8	-13.5
M6T3	-20.4	-27.2	-42.3	-51.6	-7.8	-11.8
D2T	-43.4	-54.7	-78.5	-78.9	-20.0	-31.2
D3T	-27.5	-39.2	-79.8	-87.2	-3.7	-13.2
D4T	-17.9	-24.8	-75.3	-76.7	4.6	-1.9
D5T	-8.0	-13.1	-76.4	-74.0	14.7	9.0
D6T1	-20.8	-35.7	-72.7	-86.6	0.8	-9.9
D6T2	-24.6	-39.9	-82.2	-94.2	-0.1	-11.8
D6T3	-21.8	-40.1	-90.6	-97.5	5.3	-11.0

evinced by the negative entropy changes (vide infra).

Table 1 contains the enthalpy, entropy, and Gibbs free energy changes upon adsorption of the first and second molecules of ethylene over the active sites of the NiMCM-41 catalyst where the thermodynamic data for the formation of the D*x*T sites were obtained by taking into account the collective changes in Eqs. (1) and (2). Adsorption on all of the sites was accompanied by a decrease in entropy as expected. As also evident, the monomeric adsorption of ethylene on all sites was exothermic with the most favorable adsorption occurring on the 4T cluster sites (-35.7 kcal mol^{-1} at L2) followed by M5T and M2T, both with the enthalpies of -32.4 kcal mol^{-1}. On the other hand, M6T1 showed the least exothermicity (-23.9 kcal mol^{-1} at L2). The enthalpies might be compared against the theoretically estimated adsorption energies of -28.7 kcal mol^{-1} on Ni-SSZ-24 [21].

The same trend was true for the case of free energy changes such that all of the sites adsorbed the first ethylene molecule spontaneously. The free energy values (-23.0 to -9.2 kcal mol^{-1} at L2) were mostly smaller than the value (-12.9 kcal mol^{-1}) predicted theoretically for the ethylene adsorption on the Ni-SSZ-24 zeolite [21]. More strictly, the formation of M4T, M5T and M2T π complexes in NiMCM-41 was more favorable thermodynamically than the corresponding complex on a model Ni-SSZ-24 catalyst. The adsorption of the second molecule was also found to be exothermic on all sites except 4T and 5T with both of the methods (compare the

enthalpy pairs of the dimeric and monomeric structures in Table 1). However, the whole process of dimeric adsorption was exothermic on all of the sites (-54.7 to -13.1 kcal mol^{-1} of enthalpy change at L2). In other words, the ethylene molecules were chemisorbed on all sites with the lowest amount of adsorption heat evolved on 5T. The dimeric adsorption of ethylene was most favorable on 2T (ΔG_{ads} = -31.2 kcal mol^{-1} at L2) and quite non-spontaneous on 5T (ΔG_{ads} = 9.0 kcal mol^{-1} at L2) at the adsorption conditions of 298 K and atmospheric pressure. This indicates that the activation of the pre-catalyst through the dimeric adsorption of ethylene molecules on 5T sites requires more severe (*e.g.*, high-pressure) conditions. Otherwise, the productivity will be too small at mild conditions on conceivable catalysts containing 5T structures predominantly. However, the same properties connote to the potential for controlling the chain growth during the oligomerization reactions on such active sites. Overall, the thermodynamic favorability of the adsorption of one or two molecules of ethylene over different active sites of NiMCM-41 followed the sequence of D5T < D4T < M6T1 < D6T1 < D6T3 < M6T3 < D6T2 < M3T < D3T < M6T2 < M2T < M5T < M4T < D2T as implied from the Gibbs free energy changes. The two methods gave almost the same trends, except that L2 predicted more negative energy values compared to L1 (the free energies fall within the range of -31.2 to 9.0 kcal mol^{-1} with L2 and -20.0 to 14.7 kcal mol^{-1} with L1). The vast range of Gibbs free energies obtained here can be compared against the magnitude of -5.3 kcal mol^{-1} on Ni-SSZ-24 zeolite [21]. Indeed, if comparable, for all of the sites, except 4T and 5T, a dimeric π adsorption state is more favorable to form on NiMCM-41 than on Ni-SSZ-24. Further discussions of the NBO charges, geometrical features, and QTAIM assessments can be found in the supporting information. These results highlight theimportance of studying different active sites when comparing the catalytic events on transition metal incorporated catalysts.

CONCLUSIONS

In this study, initial adsorption steps in the reaction sequence of ethylene dimerization were investigated using two density functional theory methods to give comparative insights into the molecular heterogeneities in the model NiMCM-41 catalyst. Total of 14 adsorption complexes were investigated. The adsorption of an ethylene molecule was found to be spontaneous (with free energy changes of -23.0 to -9.2 kcal mol^{-1} at L2) and exothermic on all sites with the most favorable adsorption on the 4T rings (-35.7 kcal mol^{-1} at L2) followed by 5T. The adsorption enthalpies in the dimeric mode ranged from -54.7 to -13.1 kcal mol^{-1} at L2 and was most favorable on 2T (ΔG_{ads} = -31.2 kcal mol^{-1} at L2) and quite non-spontaneous on 5T (ΔG_{ads} = 9.0 kcal mol^{-1} at L2). Overall, the predictions by two methods were in agreement with each other in most of the cases; however, L2 predicted more negative energy values than L1. According to the NBO calculations, the total charge of adsorptive molecules turned into positive values through changing on average by 0.143 and 0.205 e per molecule at the L2 level after the monomeric and dimeric adsorption stages, respectively. This minimum charge transfer was observed on the 2T sites.

Ethylene adsorption also led to an elongation of the Ni-O distances, particularly with the dimeric adsorption. This change was accompanied by some lengthening of the olefinic bonds as a consequence of π complexation. The adsorption of the ethylene molecules also led to reduced O-Ni-O angles (82.5-109.8°), with the smallest change on 2T and the largest alterations on 4T and 5T. The QTAIM analysis revealed the electrostatic nature of the interactions between the nickel ion and the olefinic bond. In some cases, the nickel-surface interactions also turned into a closed-shell type. Interestingly, the most favorable sites of NiMCM-41 to form (5T and 4T), as the most reactive sites, rendered the lowest favorability for adsorption of the ethylene molecules and the lowest reactivity to the subsequent reactions as found by the HOMO-LUMO gaps and energetic data; the reverse argument was true for the 2T site. These results underlined the relevance and usefulness of the theoretical systematic investigations of the reaction steps on different active sites along with the experimental studies of transition metal incorporated catalysts.

REFERENCES

[1] Karimzadeh, R.; Ghashghaee, M.; Nouri, M., Effect of solvent dearomatization and operating conditions in steam pyrolysis of a heavy feedstock. *Energ. Fuel.* **2010**, *24*, 1899-1907, DOI: 10.1021/ef901139u.

[2] Karimzadeh, R.; Ghashghaee, M., Design of a flexible pilot plant reactor for the steam cracking process. *Chem. Eng. Technol.* **2008**, *31*, 278-286, DOI: 10.1002/ceat.200700326.

[3] Ghashghaee, M.; Karimzadeh, R., Multivariable optimization of thermal cracking severity. *Chem. Eng. Res. Des.* **2011**, *89*, 1067-1077, DOI: 10.1016/j.cherd.2010.12.002.

[4] Ghashghaee, M.; Shirvani, S., Two-step thermal cracking of an extra-heavy fuel oil: experimental evaluation, characterization, and kinetics. *Ind. Eng. Chem. Res.* **2018**, *57*, 7421-7430, DOI: 10.1021/acs.iecr.8b00819.

[5] Shirvani, S.; Ghashghaee, M., Combined effect of nanoporous diluent and steam on catalytic upgrading of fuel oil to olefins and fuels over USY catalyst. *Petrol. Sci. Technol.* **2018**, *36*, 750-755, DOI: 10.1080/10916466.2018.1445104.

[6] Jafari Fesharaki, M.; Ghashghaee, M.; Karimzadeh, R., Comparison of four nanoporous catalysts in thermocatalytic upgrading of vacuum residue. *J. Anal. Appl. Pyrol.* **2013**, *102*, 97-102, DOI: 10.1016/j.jaap.2013.03.009.

[7] Hajheidary, M.; Ghashghaee, M.; Karimzadeh, R., Olefins production from LPG *via* dehydrogenative cracking over three ZSM-5 catalysts. *J. Sci. Ind. Res.* **2013**, *72*, 760-766, DOI: http://nopr.niscair.res.in/handle/123456789/24481.

[8] Ghashghaee, M.; Karimzadeh, R., Applicability of protolytic mechanism to steady-state heterogeneous dehydrogenation of ethane revisited. *Micropor. Mesopor. Mat.* **2013**, *170*, 318-330, DOI: 10.1016/j.micromeso.2012.12.005.

[9] Ghashghaee, M.; Ghambarian, M., Methane adsorption and hydrogen atom abstraction at diatomic radical cation metal oxo clusters: first-principles calculations. *Mol. Simul.* **2018**, *44*, 850-863, DOI: 10.1080/08927022.2018.1465568.

[10] Ghashghaee, M., Predictive correlations for thermal upgrading of petroleum residues. *J. Anal. Appl. Pyrol.* **2015**, *115*, 326-336, DOI: 10.1016/j.jaap.2015.08.013.

[11] Ghashghaee, M., Heterogeneous catalysts for gas-phase conversion of ethylene to higher olefins. *Rev. Chem. Eng.* **2018**, *34*, 595-655, DOI: http://dx.doi.org/10.1515/revce-2017-0003.

[12] Ghashghaee, M.; Farzaneh, V., Nanostructured hydrotalcite-supported RuBaK catalyst for direct conversion of ethylene to propylene. *Russ. J. Appl. Chem.* **2018**, *91*, 970-974, DOI: 10.1134/S1070427218060149.

[13] Ghashghaee, M.; Shirvani, S., Catalytic transformation of ethylene to propylene and butene over an acidic Ca-incorporated composite nanocatalyst. *Appl. Catal. A-Gen.* **2019**, *569*, 20-27, DOI: https://doi.org/10.1016/j.apcata.2018.10.017.

[14] Ghashghaee, M.; Ghambarian, M., Initiation of heterogeneous Schrock-type Mo and W oxide metathesis catalysts: A quantum thermochemical study. *Comp. Mater. Sci.* **2018**, *155*, 197-208, DOI: https://doi.org/10.1016/j.commatsci.2018.08.031.

[15] Andrei, R. D.; Popa, M. I.; Fajula, F.; Hulea, V., Heterogeneous oligomerization of ethylene over highly active and stable Ni-AlSBA-15 mesoporous catalysts. *J. Catal.* **2015**, *323*, 76-84, DOI: 10.1016/j.jcat.2014.12.027.

[16] Ghambarian, M.; Azizi, Z.; Ghashghaee, M., Diversity of monomeric dioxo chromium species in Cr/silicalite-2 catalysts: A hybrid density functional study. *Comp. Mater. Sci.* **2016**, *118*, 147-154, DOI: 10.1016/j.commatsci.2016.03.009.

[17] Finiels, A.; Fajula, F.; Hulea, V., Nickel-based solid catalysts for ethylene oligomerization- a review. *Catal. Sci. Technol.* **2014**, *4*, 2412-2426, DOI: 10.1039/c4cy00305e.

[18] Alvarado Perea, L.; Wolff, T.; Veit, P.; Hilfert, L.; Edelmann, F. T.; Hamel, C.; Seidel-Morgenstern, A., Alumino-mesostructured Ni catalysts for the direct conversion of ethene to propene. *J. Catal.* **2013**, *305*, 154-168, DOI: http://dx.doi.org/10.1016/j.jcat.2013.05.007.

[19] Ikeda, K.; Kawamura, Y.; Yamamoto, T.; Iwamoto, M., Effectiveness of the template-ion exchange

method for appearance of catalytic activity of Ni-MCM-41 for the ethene to propene reaction. *Catal. Commun.* **2008**, *9*, 106-110, DOI: 10.1016/j.catcom.2007.05.032.

[20] Tanaka, M.; Itadani, A.; Kuroda, Y.; Iwamoto, M., Effect of pore size and nickel content of Ni-MCM-41 on catalytic activity for ethene dimerization and local structures of nickel ions. *J. Phys. Chem. C* **2012**, *116*, 5664-5672, DOI: 10.1021/jp2103066.

[21] Brogaard, R. Y.; Olsbye, U., Ethene oligomerization in Ni-containing zeolites: Theoretical discrimination of reaction mechanisms. *ACS Catal.* **2016**, *6*, 1205-1214, DOI: 10.1021/acscatal.5b01957.

[22] Ghambarian, M.; Ghashghaee, M.; Azizi, Z., Coordination and siting of Cu^+ ion adsorbed into silicalite-2 porous structure: A density functional theory study. *Phys. Chem. Res.* **2017**, *5*, 135-152, DOI: http://dx.doi.org/10.22036/pcr.2017.39255.

[23] Ghambarian, M.; Azizi, Z.; Ghashghaee, M., Cluster modeling and coordination structures of Cu^+ ions in Al-incorporated Cu-MEL catalysts- a density functional theory study. *J. Mex. Chem. Soc.* **2017**, *61*, 1-13, DOI: 10.29356/jmcs.v61i1.122.

[24] Ghambarian, M.; Azizi, Z.; Ghashghaee, M., Saturated five-membered N,B-heterocyclic carbene: A computational study. *Chem. Lett.* **2015**, *44*, 1586-1588, DOI: 10.1246/cl.150660.

[25] Azizi, Z.; Ghambarian, M.; Rezaei, M. A.; Ghashghaee, M., Saturated N,X-heterocyclic carbenes (X = N, O, S, P, Si, C and B): Stability, nucleophilicity and basicity. *Aust. J. Chem.* **2015**, *68*, 1438-1445, DOI: http://dx.doi.org/10.1071/CH14715.

[26] Balar, M.; Azizi, Z.; Ghashghaee, M., Theoretical identification of structural heterogeneities of divalent nickel active sites in NiMCM-41 nanoporous catalysts. *J. Nanostruct. Chem.* **2016**, *6*, 365-372, DOI: 10.1007/s40097-016-0208-z.

[27] Ghashghaee, M.; Ghambarian, M.; Azizi, Z., Characterization of extraframework Zn^{2+} cationic sites in silicalite-2: A computational study. *Struct. Chem.* **2016**, *27*, 467-475, DOI: 10.1007/s11224-015-0575-y.

[28] Becke, A. D., Density-functional thermochemistry. III. The role of exact exchange. *J. Chem. Phys.* **1993**, *98*, 5648-5652, DOI: http://dx.doi.org/10.1063/1.464913.

[29] Zhao, Y.; Truhlar, D. G., The M06 suite of density functionals for main group thermochemistry, thermochemical kinetics, noncovalent interactions, excited states, and transition elements: two new functionals and systematic testing of four M06-class functionals and 12 other functionals. *Theor. Chem. Acc.* **2008**, *120*, 215-241, DOI: 10.1007/s00214-007-0310-x.

[30] Frisch, M. J.; Pople, J. A.; Binkley, J. S., Self-consistent molecular orbital methods 25. Supplementary functions for Gaussian basis sets. *J. Chem. Phys.* **1984**, *80*, 3265-3269, DOI: http://dx.doi.org/10.1063/1.447079.

[31] Weigend, F., Accurate coulomb-fitting basis sets for H to Rn. *Phys. Chem. Chem. Phys.* **2006**, *8*, 1057-1065, DOI: 10.1039/b515623h.

[32] Ghashghaee, M.; Shirvani, S.; Ghambarian, M., Kinetic models for hydroconversion of furfural over the ecofriendly Cu-MgO catalyst: An experimental and theoretical study. *Appl. Catal. A-Gen.* **2017**, *545*, 134-147, DOI: 10.1016/j.apcata.2017.07.040.

[33] Firouzbakht, M.; Zhou, S.; González-Navarrete, P.; Schlangen, M.; Kaupp, M.; Schwarz, H., Metal-dependent strengthening and weakening of M-H and M-C bonds by an Ooxo ligand: Thermal gas-phase activation of methane by $[OMH]^+$ and $[MH]^+$ (M=Mo, Ti). *Chem.-Eur. J.* **2017**, *23*, 12346-12352, DOI: 10.1002/chem.201701615.

[34] McLean, A. D.; Chandler, G. S., Contracted Gaussian basis sets for molecular calculations. I. Second row atoms, Z = 11-18. *J. Chem. Phys.* **1980**, *72*, 5639-5648, DOI: http://dx.doi.org/10.1063/1.438980.

[35] Valiev, M.; Bylaska, E. J.; Govind, N.; Kowalski, K.; Straatsma, T. P.; Van Dam, H. J. J.; Wang, D.; Nieplocha, J.; Apra, E.; Windus, T. L.; de Jong, W. A., NWChem: A comprehensive and scalable open-source solution for large scale molecular simulations. *Comput. Phys. Commun.* **2010**, *181*, 1477-1489, DOI: 10.1016/j.cpc.2010.04.018.

[36] Lu, T.; Chen, F., Multiwfn: A multifunctional wavefunction analyzer. *J. Comput. Chem.* **2012**, *33*, 580-592, DOI: 10.1002/jcc.22885.

[37] Macrae, C. F.; Bruno, I. J.; Chisholm, J. A.;

Edgington, P. R.; McCabe, P.; Pidcock, E.; Rodriguez-Monge, L.; Taylor, R.; van de Streek, J.; Wood, P. A., Mercury CSD 2.0 - new features for the visualization and investigation of crystal structures. *J. Appl. Crystallogr.* **2008**, *41*, 466-470, DOI: 10.1107/S0021889807067908.

[38] Yang, J. C.; Shul, Y. G.; Louis, C.; Che, M., In situ EXAFS study of the nucleation and crystal growth of Ni particles on SiO_2 support. *Catal. Today* **1998**, *44*, 315-325, DOI: http://dx.doi.org/10.1016/S0920-5861(98)00205-3.

[39] Clause, O.; Bonneviot, L.; Che, M.; Dexpert, H., EXAFS characterization of the adsorbed state of Ni(II) ions in Ni/SiO_2 materials prepared by deposition-precipitation. *J. Catal.* **1991**, *130*, 21-28, DOI: http://dx.doi.org/10.1016/0021-9517(91)90088-L.

[40] Allen, H. C.; Plyler, E. K., The structure of ethylene from infrared spectra. *J. Am. Chem. Soc.* **1958**, *80*, 2673-2676, DOI: 10.1021/ja01544a021.

[41] Medvedev, M. G.; Bushmarinov, I. S.; Sun, J.; Perdew, J. P.; Lyssenko, K. A., Density functional theory is straying from the path toward the exact functional. *Science* **2017**, *355*, 49-52, DOI: 10.1126/science.aah5975.